

---

# SpikeProphecy: A Large-Scale Benchmark for Autoregressive Neural Population Forecasting

---

John R. Minnick<sup>1,2,\*</sup>, Jinghui Geng<sup>2,3</sup>, Kamran Hussain<sup>4</sup>,  
Jesus Gonzalez-Ferrer<sup>2,5</sup>, Ash Robbins<sup>1,2</sup>, Mohammed A. Mostajo-Radji<sup>2</sup>,  
David Haussler<sup>2,5</sup>, Jason K. Eshraghian<sup>1</sup>, Mircea Teodorescu<sup>1,2,5</sup>

<sup>1</sup>Department of Electrical and Computer Engineering, University of California, Santa Cruz, CA, USA

<sup>2</sup>UC Santa Cruz Genomics Institute, University of California, Santa Cruz, CA, USA

<sup>3</sup>Department of Computer Science and Engineering, University of California, Santa Cruz, CA, USA

<sup>4</sup>Department of Applied Mathematics, University of California, Santa Cruz, CA, USA

<sup>5</sup>Department of Biomolecular Engineering, University of California, Santa Cruz, CA, USA

## Abstract

Neural population models, which predict the joint firing of many simultaneously recorded neurons forward in time, are typically evaluated by a single aggregate Pearson correlation  $r$  between predicted and actual spike counts, a number that masks critical structure. We argue that how we evaluate spike forecasting matters as much as what we build, and introduce SpikeProphecy, the first large-scale benchmark for causal, autoregressive spike-count forecasting on real electrophysiology recordings. Our core contribution is a population metric decomposition that separates aggregate performance into temporal fidelity, spatial pattern accuracy, and magnitude-invariant alignment. The decomposition surfaces aspects of the underlying data that an aggregate scalar collapses together. We apply the protocol to 105 Neuropixels sessions (Steinmetz 2019 + IBL Repeated Site; ~89,800 neurons) with seven architecture baselines spanning four structural families: four SSMs (three diagonal and one non-diagonal), a Transformer, an LSTM, and a spiking network. The decomposition surfaces a brain-region predictability ranking that reproduces across all seven baselines and survives ANCOVA correction for firing-statistics constraints (region  $\Delta R^2=0.018$  above the firing-statistics covariates). It also exposes a sub-Poisson evaluation floor where rigorous metrics combine with genuine biophysical constraints on regular spike trains, and yields a negative result on KL-on-output-rates distillation for ANN→SNN transfer in this Poisson count domain.

## 1 Introduction

High-density electrode probes such as Neuropixels record the simultaneous spiking activity of hundreds to thousands of neurons in behaving animals. A growing class of sequence models, which we collectively call *neural population models*, has been trained on these recordings using modern architectures borrowed from language and time-series work [Pandarinath et al., 2018, Ye and Pandarinath, 2021, Azabou et al., 2023]. These models are overwhelmingly evaluated on a single downstream task, *behavioral decoding*: mapping spikes to cursor velocity, stimulus identity, or movement direction. The more fundamental computational challenge is *spike forecasting*: predicting the future firing of thousands of neurons from their own recent history. This task matters for closed-loop brain-computer interfaces (BCIs), where 50–100 ms look-ahead predictions compensate for sensing and processing delays, and for *in silico* neural population simulators (“digital twins”) that

---

\*Correspondence: jrminnic@ucsc.edu

could accelerate BCI algorithm development without animal experimentation. Despite this importance, **no established benchmark exists** for spike-count forecasting at scale on real electrophysiology data.

Standard evaluation practices compound this gap. The community relies on aggregate per-neuron Pearson  $r$  as the primary metric, but a single number hides several axes: brain region differences in predictability, neuron subpopulation failures, and the distinction between temporal dynamics capture and spatial pattern fidelity. An aggregate  $r = 0.50$  sounds reasonable, but decomposing it reveals that temporal population dynamics are well-captured ( $r_{\text{pop}} = 0.76$ ) while individual neuron spatial identity is only moderately captured ( $r_{\text{spatial}} = 0.55$ ). We need *population-level metrics* that measure what actually matters for downstream applications.

We introduce the **SpikeProphecy benchmark**, designed to address both gaps simultaneously. Our contributions are:

1. **Evaluation protocol (primary contribution).** A population-metric decomposition (`pop_rate_r` for temporal fidelity, `spatial_r` for spatial pattern, `cosine_sim` for magnitude-invariant alignment) that exposes structure invisible to aggregate Pearson  $r$ . The decomposition re-orders the brain-region predictability hierarchy (§4.1), exposes a sub-Poisson evaluation floor (§4.1), and separates the failure modes of the linear-vs.-deep modeling hierarchy (§4.2) that are all missed by single- scalar reporting. We argue the decomposition should become standard for neural population forecasting (§3.3).
2. **Task & data.** The first large-scale autoregressive spike-count forecasting benchmark: 105 sessions from two public Neuropixels datasets (~89,800 neurons), with standardized preprocessing, temporal splits, and a 14-test data-integrity audit suite covering 5 leakage vectors.
3. **Seven evaluated architectures.** Four SSMs spanning the diagonal/non-diagonal axis (Mamba, HGRN2, LRU: diagonal; GatedDeltaNet: non-diagonal), a Transformer, an LSTM, and a recurrent spiking network (RSynaptic SNN), all trained under identical optimizer, schedule, loss, and data so that decomposition findings can be attributed to the task and data rather than to any single architecture choice. Per-architecture results are reported in §4 and Table 3.
4. **Findings enabled by the benchmark.** The protocol’s stratified reporting surfaces structure that standard aggregate metrics smooth over: a brain-region predictability ranking that survives ANCOVA correction (region  $\Delta R^2=0.018$  above firing-statistics covariates), a sub-Poisson evaluation floor that combines biophysical hardness with metric harshness, and a controlled negative result for KL-on-output-rates distillation in this Poisson count setting (we do not claim the result generalizes to feature-level or attention-transfer distillation).
5. **Public ecosystem.** Processed tensors and preprocessing code (the source recordings remain at their public Figshare/IBL repositories), pip-installable evaluation toolkit, trained checkpoints, and YAML reproduction configs.

## 2 Related work

**Neural population models.** LFADS [Pandarinath et al., 2018] uses a sequential VAE to estimate firing rates but targets latent dynamics inference, not forecasting. NDT/NDT2 [Ye and Pandarinath, 2021] applies masked attention to neuronal spiking for behavioral decoding. BRAID [Vahidi et al., 2025] is closest to our work (input-driven RNNs with a forecasting objective on Steinmetz recordings) but provides no multi-architecture comparison, no cross-dataset evaluation, and no population-level metrics. POCO [Duan et al., 2025] addresses neural forecasting but on calcium imaging (continuous fluorescence), not discrete spike counts, making it a fundamentally different data modality.

**Why not foundation models as baselines?** Recent neural foundation models (POYO/POYO-2, NDT-2, brain2vec) are not drop-in comparisons: each was pretrained for a different task (masked-token prediction, latent inference, session-level embeddings) and would require substantial adaptation to produce causal 50 ms-bin rate forecasts (Appendix A.1). We acknowledge this absence as a real gap; our architecture-level findings cannot claim state-of-the-art.

**Neural data benchmarks.** The Neural Latents Benchmark (NLB; Pei et al. 2021) standardized evaluation of latent variable models using co-smoothing bits per spike (co-BPS) on 4 motor/cognitive datasets. NLB targets *latent inference* (unsupervised rate smoothing), whereas SpikeProphecy targets *causal forecasting* of future spike counts from history alone. NeuroBench [Yik et al., 2025] benchmarks neuromorphic algorithms but on classification tasks (keyword spotting, event vision),

not neural time-series. SpikeProphecy bridges this gap: the first benchmark for autoregressive spike prediction at scale, with evaluation metrics that decompose performance beyond scalar summaries. Table 4 contrasts our evaluation protocol with existing practice.

**Sequence architectures for neural data.** Structured state-space models (S4, S5) and their successors (Mamba [Gu and Dao, 2023], LRU [Orvieto et al., 2023]) have shown strong performance on long-range sequence tasks. We provide the first systematic comparison of these architectures on neural spike data, including evaluation beyond Pearson  $r$ .

**Evaluation methodology.** Standard neural data metrics (per-neuron  $r$ , co-BPS,  $R^2$ ) are all aggregate scalar summaries that collapse temporal and spatial fidelity into a single number. HELM [Liang et al., 2022] demonstrated in the LLM domain that multi-axis evaluation (accuracy  $\times$  fairness  $\times$  calibration) reveals trade-offs invisible to single-metric leaderboards. Our population-level metrics bring this philosophy to neuroscience, inspired by population vector analysis [Georgopoulos et al., 1986] but applied to forecast evaluation.

**ANN-to-SNN distillation.** Knowledge distillation for spiking networks [Hong et al., 2025] has been studied exclusively on image classification (CIFAR, ImageNet). No prior work evaluates ANN-to-SNN distillation on spike forecasting; our negative result is the first empirical demonstration, with a hypothesized mechanism (the redundancy of soft labels when the target is already real-valued), for why standard KL-weighted distillation fails in Poisson regression domains.

### 3 Benchmark design

#### 3.1 Task formulation

Given a history window of  $T$  spike-count vectors, predict the next time bin:

$$X_t = \{\mathbf{x}(t-T+1), \dots, \mathbf{x}(t)\} \longrightarrow \hat{\mathbf{y}}(t+1) \approx \mathbf{x}(t+1), \quad \mathbf{x}(t) \in \mathbb{Z}_{\geq 0}^M \quad (1)$$

where  $M$  is the number of simultaneously recorded neurons in a session (varies between sessions, up to  $M_{\max}=1,998$  in the largest IBL session),  $\Delta t = 50$  ms, and  $T = 10$  bins (500 ms history). Sessions are zero-padded to  $M_{\max}$  with a per-sample binary channel mask; the loss operates only on real channels. The model outputs softplus rates  $\hat{\lambda}_i > 0$  trained with Poisson NLL. Two constraints define the task: *strictly autoregressive* (intrinsic covariates only: past spikes, no stimulus/behavioral features) and *causal* (no future context at any layer). This rules out stimulus information unavailable at BCI inference time and the bidirectional attention used in masked-token foundation models like POYO/NDT-2.

#### 3.2 Datasets

**Steinmetz 2019 (39 sessions).** Ten mice, 39 recording sessions using Neuropixels probes spanning visual cortex, motor cortex, hippocampus, thalamus, and midbrain [Steinmetz et al., 2019]. Up to 1,240 simultaneously recorded neurons per session. Visual discrimination task (~2-hour recordings). Single lab, single rig, controlled conditions. Source data are publicly available on Figshare under CC-BY-4.0 (<https://doi.org/10.6084/m9.figshare.9598406.v2>); our processed 50 ms-binned tensors plus per-session metadata (split boundaries, brain-region labels) are released as a HuggingFace dataset (<https://huggingface.co/datasets/mysteriousauthor/spikeprophecy-steinmetz>).

**IBL Repeated Site (66 sessions).** Multi-lab international consortium, standardized probe trajectory across 9 labs [Laboratory et al., 2025]. Up to 1,998 simultaneously recorded neurons. Same task paradigm across different labs, mice, and rigs; tests cross-lab generalization. Source data are publicly available via the IBL Open Neurophysiology Environment ONE API (<https://www.internationalbrainlab.com/data>); as above, we redistribute only the processed tensors and the preprocessing pipeline.

**Processing and splits.** Raw spike times are binned at 50 ms into integer count vectors. Each session is split temporally into three contiguous blocks (70/15/15 train/val/test, ordered first/middle/last in time) to prevent information leakage. Interleaved or random splits would introduce trivial leakage on autoregressive forecasting because adjacent 50 ms bins are temporally correlated.

**Auditable leakage suite.** We ship a 14-test audit suite that runs on every commit and verifies five leakage vectors (Appendix A.3). The Population-GLM result in Table 3 ( $r=1.000$  on train,  $r=-0.015$  on val) is the canonical catch.

### 3.3 Evaluation protocol: population metric decomposition

Each of the three metrics below is individually well-precedented (population vector analysis [Georgopoulos et al., 1986], per-bin cross-neuron correlation, magnitude-invariant cosine alignment); our contribution is standardizing the triplet as the reporting protocol for spike-count forecasting and showing empirically (§4.1) that it surfaces structure aggregate  $r$  hides. The three describe distinct axes (one marginalizes neurons, one marginalizes time, one removes magnitude); they are not orthogonal components of an algebraic identity summing to  $Wt-r$ .

**Standard metrics (baseline protocol).** Existing benchmarks rely on aggregate Pearson  $r$  (*weighted Pearson  $r$ ,  $Wt-r$* ), per-neuron median  $r$ , co-smoothing bits per spike (co-BPS), Poisson NLL, and mean absolute error (MAE) – all scalar summaries that conflate temporal and spatial fidelity (Appendix A.5 contrasts the protocols). We define  $Wt-r$  as the activity-weighted mean of per-neuron Pearson correlations:

$$Wt-r = \frac{\sum_{i=1}^M w_i \cdot \text{Pearson}(y_i, \hat{y}_i)}{\sum_{i=1}^M w_i}, \quad w_i = \text{Var}(y_i), \quad (2)$$

where weighting downweights near-silent neurons.  $Wt-r$  is the headline metric in Table 3, reported for backwards comparability.

**Population metric decomposition (our contribution).** Let  $\mathbf{y}(t), \hat{\mathbf{y}}(t) \in \mathbb{R}^M$  denote ground-truth and predicted activity vectors at time bin  $t$  across  $M$  neurons and  $T_{\text{eval}}$  evaluation bins.

(i) **Population Rate  $r$  (pop\_rate\_r).** Temporal fidelity: *when is the population active?*

$$r_{\text{pop}} = \text{Pearson}\left(\left[\sum_{i=1}^M y_i(t)\right]_{t=1}^T, \left[\sum_{i=1}^M \hat{y}_i(t)\right]_{t=1}^T\right) \quad (3)$$

Marginalizes over neuron identity to measure ensemble rate envelope tracking.

(ii) **Spatial Pattern  $r$  (spatial\_r).** Spatial fidelity: *which neurons fire?*

$$r_{\text{spatial}} = \frac{1}{T_{\text{eval}}} \sum_{t=1}^{T_{\text{eval}}} \text{Pearson}(\mathbf{y}(t), \hat{\mathbf{y}}(t)) \quad (4)$$

Per-timebin cross-neuron correlation, capturing identification of the active subset at each moment.

(iii) **Population Cosine Similarity (cosine\_sim).** Magnitude-invariant pattern alignment: *relative activation regardless of overall rate?*

$$\text{cos\_sim} = \frac{1}{T_{\text{eval}}} \sum_{t=1}^{T_{\text{eval}}} \frac{\mathbf{y}(t) \cdot \hat{\mathbf{y}}(t)}{\|\mathbf{y}(t)\| \|\hat{\mathbf{y}}(t)\|} \quad (5)$$

Normalizing magnitudes isolates pattern fidelity from rate calibration. Because spike counts and softplus predictions are non-negative, cosine here lives in the positive orthant and has a non-zero floor: train-set-mean reaches  $\text{cos} = 0.31$  (empirical floor), the autoregressive GLM 0.24, the modern-recurrence cluster 0.61–0.63, the trailing baselines  $\text{cos} \approx 0.58$  (Table 3). The dynamic range 0.31–0.63 remains discriminative.

We additionally advocate reporting results *stratified* by brain region (§4.1) and Fano factor class (§4.1).

### 3.4 Architecture baselines

All architectures share input pipeline, loss, optimizer, and training schedule (50 epochs, AdamW, cosine LR with warmup, seed=42; full per-arch hyperparameters in Appendix A.4).

Table 1: Architecture baselines in the SpikeProphecy benchmark. All models use shared output heads and identical training hyperparameters.

Architecture	Type	Params	Key property
Mamba	Diagonal selective SSM	1.95M	Input-dependent gating, $O(T)$
HGRN2	Diagonal gated linear RNN	1.82M	State expansion, $O(T)$
LRU	Diagonal linear recurrence	1.23M	Ring eigenvalue init
GatedDeltaNet	Non-diagonal delta-rule SSM	1.43M	Matrix state per head, $O(T)$
Transformer	Causal attention	2.22M	Global context, $O(T^2)$
LSTM	Gated recurrence	2.22M	Classical baseline
SNN	Spiking (RSynaptic)	965K	Event-driven, neuromorphic (3L)
Autoreg GLM	Poisson, own $T$ -step hist.	$\sim 10/N$	No cross-neuron info
Population GLM	Poisson, full $(T, M)$ hist.	$\sim 7K/N$	Linear pop baseline

## 4 Results

### 4.1 Decomposition reveals structure invisible to aggregate $r$

The population metric decomposition and stratified evaluation reveal two findings that are **invisible to standard aggregate metrics**. Each demonstrates structure that would be missed by reporting a single Pearson  $r$ .

**Finding 1: A functional brain-region predictability hierarchy.** Parsing Allen CCF brain region labels for 27,212 neurons across 39 sessions reveals a predictability hierarchy that remains significant after ANCOVA correction for log firing rate and Fano factor (Figure 2a). The full ANCOVA model ( $\text{model}_r \sim \log\_rate + \text{fano} + \text{region}$ ) reaches  $R^2=0.275$  at the 8-system grouping; the covariates alone reach  $R^2=0.257$ , so the *region-incremental* contribution beyond firing-statistics is  $\Delta R^2=0.018$  at this granularity. The increment is modest but reproducible: it survives ANCOVA correction (partial  $F > 10^2$ ,  $p < 10^{-77}$ ) and is robust to grouping choice. At a coarser 4-class grouping (Cortex/Subcortex/Hippocampal/Other) the increment drops to  $\Delta R^2=0.011$ ; at the fine 54-region Allen acronym level it rises to  $\Delta R^2=0.053$  (Appendix A.11). As Figure 2a shows, the ranking itself is reproducible across all seven baselines: every architecture traces the same monotonic hierarchy across the eight functional regions despite their absolute-level differences, which is the more substantive finding than the absolute  $R^2$ . The uncorrected Kruskal–Wallis statistic ( $H=1,056$ ,  $p < 10^{-200}$ ) is inflated by the large neuron count and should not be interpreted as an effect size.

Table 2: **Finding 1: Brain-region predictability hierarchy** (Mamba per-neuron Pearson  $r$ , val split; 21,689 of 27,212 Steinmetz neurons assigned to one of 8 Allen CCF functional systems). This ranking is hidden by aggregate  $r$  and persists after ANCOVA correction for firing rate and Fano factor (Figure 2a).  $\bar{r}$ : mean per-neuron Pearson  $r$ ; %sub-P: fraction with Fano factor  $< 1$ .

Region group	$N$	Mean $r$	%sub-P
Motor cortex	1,780	<b>0.175</b>	25%
Thalamus	5,240	0.170	11%
Midbrain/Brainstem	3,440	0.168	42%
Sensory cortex	2,838	0.156	28%
Frontal/Association	2,507	0.153	34%
Hippocampal	3,736	0.130	23%
Basal ganglia	1,689	0.121	49%
Limbic/Other	459	0.080	22%

This hierarchy **survives** ANCOVA controlling for log firing rate and Fano factor ( $R^2=0.275$ ,  $\Delta R^2=0.018$  above the firing-statistics covariates,  $p < 10^{-77}$ ), supporting its interpretation as a property of the regions themselves rather than of firing statistics alone. The ranking is also stable across the seven baselines we tested (Mamba, HGRN2, Transformer, GatedDeltaNet, LRU, LSTM, SNN); we frame this as a within-recipe consistency check rather than as evidence of architecture-independence in the strong sense, since these baselines share an optimizer, schedule, loss, and training data. Stimulus-driven regions (motor, midbrain) exhibit highly predictable 50 ms dynamics, while

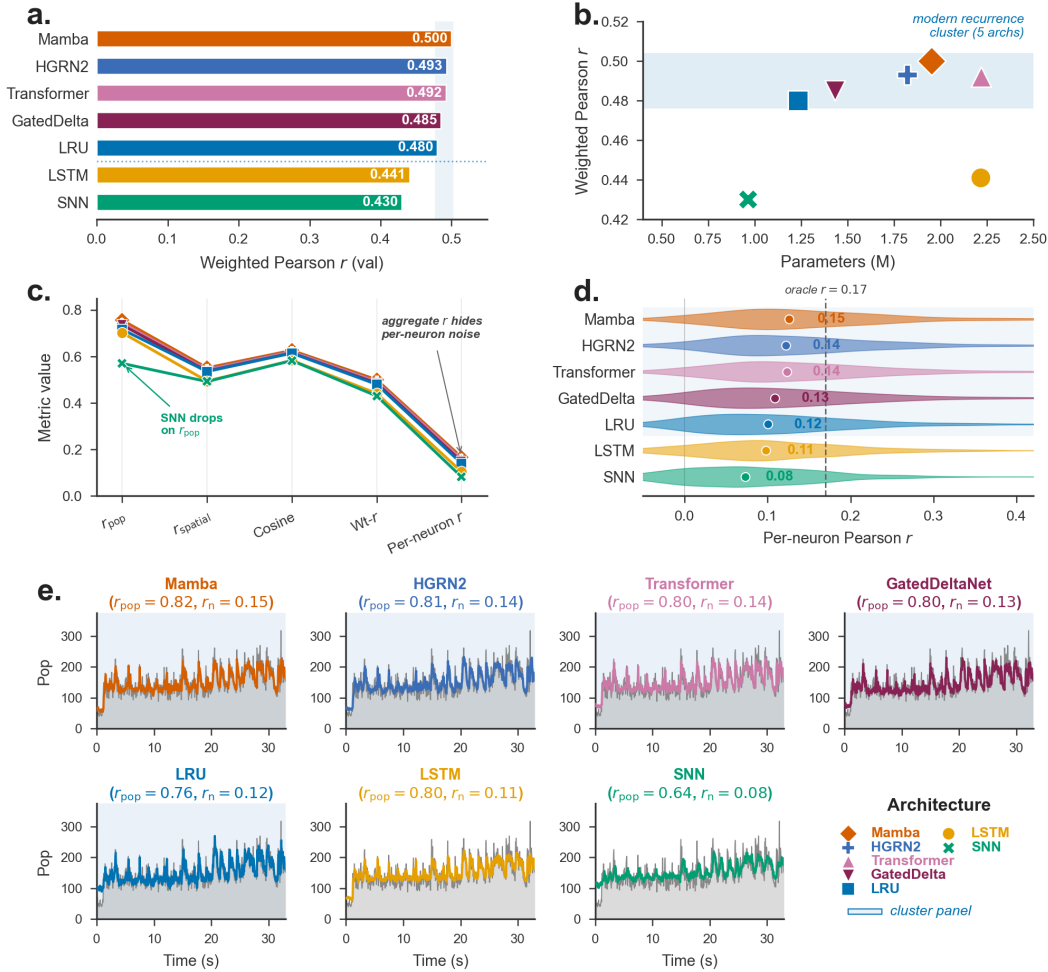


Figure 1: **SpikeProphecy benchmark overview.** Per-arch color/marker is consistent across (a)–(e). (a)–(d) summarize all 39 Steinmetz sessions (27,212 neurons); (e) shows predictions on near-median session 4. **(a)** Absolute Wt- $r$ , sorted: five cluster baselines fall in 0.480–0.500 (blue band), LSTM 0.441, SNN 0.430; dotted divider marks the Wilcoxon-significant cluster-vs.-LSTM/SNN gap ( $p < 10^{-7}$ ). **(b)** Pareto: Wt- $r$  vs. parameter count. **(c)** Decomposition trace across five normalized metrics: cluster archs overlap; SNN drops on  $r_{\text{pop}}$ ; per-neuron  $r$  collapses an order of magnitude below the aggregate metrics for every architecture. **(d)** Per-neuron  $r$  violins ( $\sim 700$  neurons of session 4). Empirical oracle ceiling ( $r = 0.17$ , dashed). **(e)** Population-rate small multiples on a near-median Steinmetz session ( $N = 703$ ,  $\sim 33$  s); cluster panels carry a faint blue background; titles report session-4  $r_{\text{pop}}$  and per-neuron  $r_n$ .

memory/association regions (hippocampus) have internally-generated dynamics operating on longer timescales than our 500 ms context, identifying a concrete target for future model development.

**Finding 2: A sub-Poisson evaluation floor with two compounding causes.** 28% of neurons have Fano factor  $< 1$  (more regular than Poisson). These regular-firing neurons are the **hardest** to predict across *all* architectures tested (mean  $r = 0.073$  vs. 0.151 for super-Poisson neurons; Figure 2b). Part of this gap is biophysical (the model lacks the relevant within-neuron oscillator covariate) and part is a metric artifact (Pearson punishes timing jitter quadratically in low-variance regimes); the two contributions are entangled in this measurement. Why are clock-like neurons so hard to forecast? Two compounding reasons. First, sub-Poisson regularity reflects intrinsic oscillatory or pacemaker dynamics driven by single-cell biophysics rather than by the population history available to the model on a 50 ms timescale, so the model lacks the relevant covariate. Second, when a neuron’s true count distribution has very low variance, even small phase mispredictions translate into large per-bin

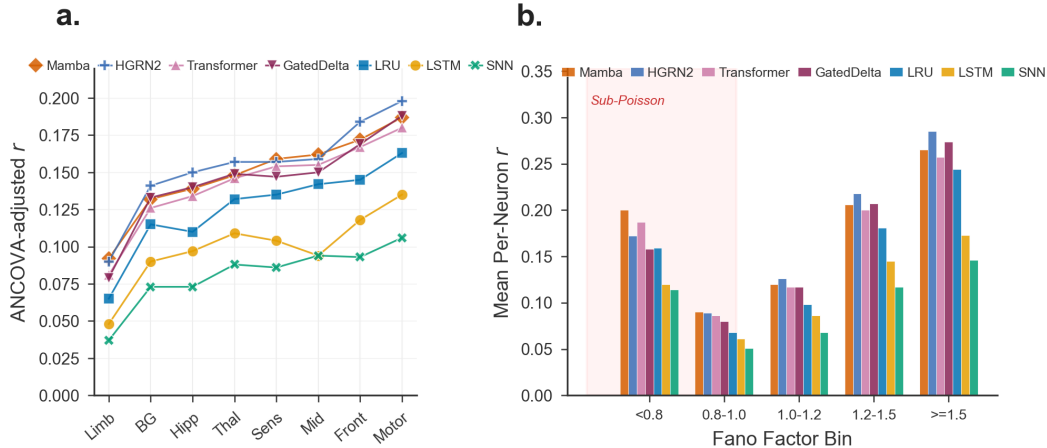


Figure 2: **Findings enabled by the population metric decomposition.** (a) ANCOVA-adjusted per-neuron  $r$  across 8 functional brain regions (39-session aggregate, 27,212 neurons), one line per architecture. Covariates: log mean firing rate + Fano factor. All seven baselines trace the same monotonic hierarchy across regions despite their absolute-level differences, indicating the predictability ranking is a property of the data, not of any single architecture. Motor cortex and midbrain are easiest; Limbic/Other and Hippocampal are hardest. Cluster archs occupy the upper band (Mamba, HGRN2, Transformer, GatedDeltaNet, LRU); LSTM and SNN sit visibly below at every region. (b) Per-neuron  $r$  by Fano factor bin across all seven baselines (39-session aggregate, val split, 26,631 neurons binned). The  $0.8 \leq FF < 1.0$  sub-Poisson bin is the lowest for *every* architecture, a fundamental evaluation ceiling that standard aggregate  $r$  conceals.

Pearson penalties: the metric punishes timing jitter quadratically in a low-variance regime. These neurons therefore impose a **hard noise floor** on aggregate metrics:  $\sim 0.07$  regardless of model quality. This has a concrete reporting consequence: without Fano-stratified evaluation, a model that improves only on super-Poisson neurons (where the signal is) will look marginal on aggregate  $r$  even if its real-signal improvement is substantial.

## 4.2 Baselines and the linear bracket

The findings above were generated by running the seven architecture baselines and two GLM controls under identical training conditions. We report their relative performance here for completeness; the ranking is a consequence of the protocol, not a contribution of the paper. Table 3 gives full per-architecture results on Steinmetz 2019 (39 sessions, 27,212 neurons).

All seven baselines surface the same structural findings under our shared training recipe (region hierarchy, Fano stratification); this is a within-recipe consistency check, not a strong architecture-independence claim (§2).

The five modern-recurrence architectures (Mamba, HGRN2, Transformer, GatedDeltaNet, LRU) cluster within 2 percentage points ( $r=0.480$ – $0.500$ ). The within-cluster spread is on the order of per-session noise on this 39-session draw (Appendix A.9), so we report the cluster as a band rather than an ordering. The classical LSTM ( $r=0.441$ ) and depth-matched SNN ( $r=0.430$ ) fall below the cluster; the SNN ablation (Appendix A.8) recovers to  $r=0.481$  at 1 layer with 36% of the parameters.

**Trivial baselines calibrate the metric scale.** Two parameter-free baselines anchor the leaderboard at the bottom. *Persistence* (predict the previous bin) reaches  $Wt-r=-0.003$  and  $r_{\text{pop}}=0.03$ , confirming that 50 ms own-bin history carries essentially no information about the next bin. *Train-mean* (predict the per-neuron training-set mean, a constant in time) achieves  $Wt-r=0$  and  $r_{\text{pop}}=0$  by construction but reaches  $\text{cos}=0.31$ , which is the true positive-orthant floor for cosine on non-negative spike-count vectors; deep models reaching  $\text{cos}=0.62$ – $0.63$  doubles this floor. Persistence achieves the lowest MAE in the table (0.260, below Mamba’s 0.283), because most 50 ms bins contain zero spikes and persistence predicts zero on those bins; this confirms that MAE on this task is dominated by the rate floor and should be read alongside Pearson-based metrics rather than as a primary objective.

Table 3: Per-architecture results on Steinmetz 2019 (39 sessions, 27,212 neurons, val split). Five modern-recurrence baselines cluster at  $r=0.480\text{--}0.500$ ; LSTM and SNN fall below. Four non-deep baselines anchor the floor: *persistence* and *train-mean* calibrate, the autoregressive GLM and CV-ridge population GLM bracket the linear regime, and the fixed- $\alpha$  population GLM is included as a leakage-audit catch ( $r=-0.015$  on val). Cluster-vs.-trailing significance (Wilcoxon,  $p<10^{-7}$ ), the no-within-cluster-ordering caveat, and per-session SEs are detailed in §4.2 and Appendix A.9. CV-ridge MAE is inflated by the softplus link (Appendix A.10).

Model	Params	Wt- $r$ ↑	$r_{\text{pop}}$ ↑	$r_{\text{spat}}$ ↑	cos↑	MAE↓
<b>Mamba</b>	1.95M	<b>0.500</b>	<b>0.756</b>	<b>0.551</b>	<b>0.626</b>	<b>0.283</b>
HGRN2	1.82M	0.493	0.740	0.544	0.621	0.286
Transformer	2.22M	0.492	0.744	0.543	0.620	0.286
GatedDeltaNet	1.43M	0.485	0.735	0.537	0.615	0.288
LRU	1.23M	0.480	0.716	0.535	0.614	0.290
LSTM	2.22M	0.441	0.702	0.494	0.583	0.298
SNN (3L)	965K	0.430	0.570	0.492	0.582	0.301
Persistence	0	-0.003	0.030	0.024	0.114	0.260
Train-mean	$\sim 1/N$	0.000	0.000	0.069	0.310	0.350
Autoreg GLM	$\sim 10/N$	+0.001	0.150	0.091	0.237	0.253
Pop GLM (fixed $\alpha$ , leakage catch)	$\sim 7K/N$	-0.015	–	–	–	–
Pop GLM (CV-ridge $\alpha$ )	$\sim 7K/N$	+0.023	0.143	0.076	0.224	0.813

**Linear baselines fail for distinct reasons; deep models succeed.** Two controlled GLM baselines bracket what a linear model can do on this task. The per-neuron autoregressive GLM (each neuron’s own  $T=10$ -bin history, 10 features per model) reaches  $r \approx 0.001$  on held-out time despite fitting training data at a modest level ( $r \approx 0.17$  on a representative session), indicating that 50 ms own-history dynamics do not generalize across the temporal split; firing statistics are non-stationary within a 2-hour recording. The population GLM (full flattened  $(T, M)$  history,  $\sim 7K$  features per neuron,  $\alpha=10^{-4}$ ) achieves  $r = 1.000$  on train but  $r = -0.015$  on val. We include this configuration deliberately as the canonical leakage-suite catch (§3.2): a feature-rich linear model on a temporally-split benchmark is guaranteed to overfit under fixed regularization, and the audit suite is what flags it. A fairer linear comparison is the same architecture with  $\alpha$  tuned per session on val (grid:  $\{10, 10^2, 10^3, 10^4\}$ , picked by val mean per-neuron  $r$ ). This CV-ridge variant escapes the catastrophic overfit (Wt- $r=+0.023$  on val, vs.  $-0.015$  at fixed  $\alpha$ ) but still falls far short of deep models: per-session val mean  $r=0.027 \pm 0.005$ , comparable to the autoregressive GLM and  $\sim 20\times$  below the deep architectures. The CV-ridge population metrics ( $r_{\text{pop}}=0.14$ ,  $r_{\text{spatial}}=0.08$ ,  $\text{cos}=0.22$ ) sit in the same regime as the autoregressive GLM, not the deep cluster. Full per-session results in Appendix A.10. The finding here is a methodological one: all seven deep architectures remain stable under the same temporal split where the linear population model collapses or only marginally clears zero, achieving 3–5 $\times$  gain over the autoregressive baseline.

### 4.3 Cross-dataset scaling on the Mamba teacher (summary)

The Mamba teacher trained on the 105-session combined Steinmetz+IBL corpus reaches Wt- $r=0.556$  vs. 0.500 on Steinmetz-only (+11%), with  $r_{\text{pop}}$  and cosine gaining similarly and spatial  $r$  slightly degrading; cross-lab transfer required no architectural modification. Full table and caveats (confound between session count and channel-space size, IBL-only vs. combined qualitative comparison) are in Appendix A.7.

### 4.4 SNN baselines and teacher distillation (summary)

The best standalone SNN (1 layer, 702K parameters; 36% of Mamba’s count) matches 96% of Mamba’s Wt- $r$  and 91% of its cosine; adding depth *hurts* and no KL-on-output-rates distillation variant ( $\beta \in \{0, 0.5, 1.0\}$ ) beats standalone training. We attribute this to teacher rates carrying no “dark knowledge” advantage when targets are already real-valued. Full depth and  $\beta$  ablations + mechanism discussion in Appendix A.8; the scope-claim is *output-distillation only* (feature-level / attention transfer not tested).

## 5 Discussion

**Summary of findings.** The protocol’s three metrics plus stratified reporting (by region and Fano factor), applied to the 39-session Steinmetz benchmark with seven architecture baselines, surfaces four findings that traditional single-scalar correlation reporting would obscure:

1. **Brain-region predictability ranking, stable across the seven baselines we tested** across 8 Allen functional systems (region  $\Delta R^2=0.018$  above firing-statistics covariates, full-model  $R^2=0.275$ ,  $p<10^{-77}$ ); ANCOVA *re-orders* the ranking relative to raw means.
2. **Sub-Poisson evaluation floor:** 28% of neurons are more regular than Poisson and contribute mean  $r\approx 0.07$  regardless of model. The gap is partly biophysical (missing oscillator covariate) and partly metric-artifactual (Pearson punishes timing jitter in low-variance regimes).
3. **Linear-vs.-deep modeling hierarchy** with distinct failure modes: per-neuron autoregressive GLM ( $r\approx 0$ , non-stationary), population GLM ( $r=-0.015$ , capacity-overfit), deep models ( $r\sim 0.5$ , succeed nonlinearly).
4. **KL-on-output-rates distillation does not help in this Poisson count domain** (negative result, §4.4, Appendix A.8). The standalone 1L SNN matches 96% of the cluster-leader Wt- $r$  at 36% of the parameters; KL on softplus rates degrades performance.

**Use cases and implications.** Decomposed metrics expose deployment-relevant trade-offs aggregate  $r$  collapses: high cosine + mediocre aggregate  $r$  suits brain-state classification or coarse population-vector decoding, while strong  $r_{\text{pop}}$  + weak  $r_{\text{spatial}}$  suits population-rate tracking (seizure detection, BCI gating) but not single-neuron stimulation. The hippocampal gap ( $r = 0.10$ ) identifies a concrete target for extended-context or latent-state models, and the sub-Poisson floor motivates dispersion-aware losses (e.g., Conway–Maxwell–Poisson). A pre-registered diagonal-vs. non-diagonal SSM test was inconclusive (Appendix A.12). We propose SpikeProphecy as a reporting standard, analogous to HELM for LLMs or NLB for latent dynamics.

**Limitations.** (1) One-step ( $H=1$ ), 50 ms bins. (2) No hardware-deployed neuromorphic evaluation, no behavioral-decoding downstream task. (3) Steinmetz + IBL only (mouse Neuropixels, overlapping visual/decision tasks), so cross-dataset claims are *cross-lab within paradigm*. (4) No foundation-model baselines (POYO, NDT-2, brain2vec; see §2). (5) Three architectures are 3-seed, four are single-seed; seed variance is two orders of magnitude below per-session SE so the 39-session sample is the within-cluster bottleneck, but the cluster-vs.-LSTM/SNN gap survives both (Appendix A.9).

## 6 Release

We release processed 50 ms-binned tensors (<https://huggingface.co/datasets/mysteriousauthor/spikeprophecy-steinmetz>, CC-BY-4.0; IBL at acceptance), a `pip install spikeprophecy` evaluation toolkit (MIT), trained checkpoints for all seven architectures, and YAML reproduction configs. Maintenance plan and source-data URLs in Appendix A.15.

**Broader impacts.** Standardized evaluation infrastructure lowers entry cost for ML researchers entering computational neuroscience and the leakage-audit suite establishes a reproducibility floor. Potential negative use: spike-forecasting models could be deployed in invasive neural interfaces without sufficient additional validation; we explicitly disclaim clinical suitability. See the Croissant `rai:dataSocialImpact` field for the machine-readable version.

## References

- Mehdi Azabou, Vinam Arora, Venkataramana Ganesh, Ximeng Mao, Santosh Nachimuthu, Michael Mendelson, Blake Richards, Matthew Perich, Guillaume Lajoie, and Eva Dyer. A unified, scalable framework for neural population decoding. *Advances in Neural Information Processing Systems*, 36:44937–44956, 2023.
- Yu Duan, Hamza Tahir Chaudhry, Misha B Ahrens, Christopher D Harvey, Matthew G Perich, Karl Deisseroth, and Kanaka Rajan. Poco: Scalable neural forecasting through population conditioning. *ArXiv*, pages arXiv–2506, 2025.
- Apostolos P Georgopoulos, Andrew B Schwartz, and Ronald E Kettner. Neuronal population coding of movement direction. *Science*, 233(4771):1416–1419, 1986.

- Albert Gu and Tri Dao. Mamba: Linear-time sequence modeling with selective state spaces. *arXiv preprint arXiv:2312.00752*, 2023.
- Geoffrey Hinton, Oriol Vinyals, and Jeff Dean. Distilling the knowledge in a neural network. *arXiv preprint arXiv:1503.02531*, 2015.
- Di Hong, Yu Qi, and Yueming Wang. Lasnn: Layer-wise ann-to-snn distillation for effective and efficient training in deep spiking neural networks. *Neurocomputing*, page 131351, 2025.
- International Brain Laboratory, Kush Banga, Julius Benson, Jai Bhagat, Dan Biderman, Daniel Birman, Niccolò Bonacchi, Sebastian A Bruijns, Kelly Buchanan, Robert AA Campbell, et al. Reproducibility of in vivo electrophysiological measurements in mice. *Elife*, 13:RP100840, 2025.
- Percy Liang, Rishi Bommasani, Tony Lee, Dimitris Tsipras, Dilara Soylu, Michihiro Yasunaga, Yian Zhang, Deepak Narayanan, Yuhuai Wu, Ananya Kumar, et al. Holistic evaluation of language models. *arXiv preprint arXiv:2211.09110*, 2022.
- Antonio Orvieto, Samuel L Smith, Albert Gu, Anushan Fernando, Caglar Gulcehre, Razvan Pascanu, and Soham De. Resurrecting recurrent neural networks for long sequences. In *International conference on machine learning*, pages 26670–26698. PMLR, 2023.
- Chethan Pandarinath, Daniel J O’Shea, Jasmine Collins, Rafal Jozefowicz, Sergey D Stavisky, Jonathan C Kao, Eric M Trautmann, Matthew T Kaufman, Stephen I Ryu, Leigh R Hochberg, et al. Inferring single-trial neural population dynamics using sequential auto-encoders. *Nature methods*, 15(10):805–815, 2018.
- Felix Pei, Joel Ye, David Zoltowski, Anqi Wu, Rameed H Chowdhury, Hansem Sohn, Joseph E O’Doherty, Krishna V Shenoy, Matthew T Kaufman, Mark Churchland, et al. Neural latents benchmark’21: evaluating latent variable models of neural population activity. *arXiv preprint arXiv:2109.04463*, 2021.
- Zhen Qin, Songlin Yang, Weixuan Sun, Xuyang Shen, Dong Li, Weigao Sun, and Yiran Zhong. Hgrn2: Gated linear rnns with state expansion. *arXiv preprint arXiv:2404.07904*, 2024.
- Nicholas A Steinmetz, Peter Zatzka-Haas, Matteo Carandini, and Kenneth D Harris. Distributed coding of choice, action and engagement across the mouse brain. *Nature*, 576(7786):266–273, 2019.
- Parsa Vahidi, Omid G Sani, and Maryam M Shanechi. Braid: Input-driven nonlinear dynamical modeling of neural-behavioral data. *ArXiv*, pages arXiv–2509, 2025.
- Songlin Yang, Jan Kautz, and Ali Hatamizadeh. Gated delta networks: Improving mamba2 with delta rule. *arXiv preprint arXiv:2412.06464*, 2024.
- Joel Ye and Chethan Pandarinath. Representation learning for neural population activity with neural data transformers. *arXiv preprint arXiv:2108.01210*, 2021.
- Jason Yik, Korneel Van den Berghe, Douwe Den Blanken, Younes Bouhadjar, Maxime Fabre, Paul Hueber, Weijie Ke, Mina A Khoei, Denis Kleyko, Noah Pacik-Nelson, et al. The neurobench framework for benchmarking neuromorphic computing algorithms and systems. *Nature communications*, 16(1):1545, 2025.

## A Additional results

### A.1 Why foundation-model baselines are not included

POYO/POYO-2 [Azabou et al., 2023] tokenize individual spike events and pretrain for *masked-token prediction* across heterogeneous sessions; adapting POYO to produce a causal, 50 ms-bin rate forecast requires swapping its output head and reintroducing a temporal causality constraint that its bidirectional attention violates. NDT-2 [Ye and Pandarinath, 2021] targets *latent inference* (unsupervised smoothing of current-bin rates under co-smoothing) and is evaluated primarily on behavioral decoding; forecasting the next bin from history alone is not a supported task in the public release. brain2vec and similar representation-learning approaches produce session-level embeddings rather than per-bin rate predictions. A comparison that required retraining each of these under our causal forecasting task with matched compute and data would itself be a paper. We release our exact causal dataloaders and temporal splits so the community can adapt and benchmark foundation models on strict causal forecasting using the same substrate.

## A.2 Benchmark access and usage

SpikeProphecy is designed as a **living benchmark ecosystem**, not a static dataset release. Usage follows three steps:

1. **Load data:** `ds = load_dataset("spikeprophecy/steinmetz")`
2. **Train and predict:** Use any architecture with the provided DataLoader and Poisson NLL loss.
3. **Evaluate:** `metrics = spikeprophecy.evaluate(pred, gt)` → returns `pop_rate_r`, `spatial_r`, `cosine_sim`, stratified by region and Fano factor.

The toolkit outputs a standardized JSON report, ships a datasheet (Appendix A.15) and the leakage audit suite (Appendix A.3), and includes pre-computed baseline predictions for all seven architectures.

## A.3 Auditable leakage suite

We ship a 14-test automated audit suite that runs on every commit and verifies five concrete leakage vectors: train/test bin overlap, sliding-window boundary crossing, cross-session spillover, normalization using future statistics, and history-feature leakage. The population-GLM result reported in Table 3 ( $r=1.000$  on train,  $r=-0.015$  on val) is the canonical example of what these tests catch when a benchmark grants linear models excessive feature access on a temporally-split task. Temporal-split leakage tests are not novel in themselves; we contribute the packaged suite plus the canonical Population-GLM catch as a reusable artifact that runs on every commit. At this scale, leakage failures are statistically indistinguishable from genuine signal at  $r\sim 0.1$ , and we expect the suite to be more useful than the specific tests it currently contains.

## A.4 Architecture hyperparameters

All architectures use  $d_{\text{model}}=256$  and 3 layers, trained with AdamW + cosine LR + warmup, 50 epochs, seed=42, shared input/output projections to  $M_{\text{max}}$ .

- **Mamba** [Gu and Dao, 2023]: selective SSM with input-dependent parametrization,  $d_{\text{state}}=16$ .
- **HGRN2** [Qin et al., 2024]: gated linear RNN with state expansion, `expand_ratio=2` so  $d_{\text{state}}=512$ . Included as a second diagonal SSM control.
- **GatedDeltaNet** [Yang et al., 2024]: non-diagonal modern SSM using the gated delta rule, matrix state per head ( $n_{\text{heads}}=4$ ,  $d_{\text{head}}=64$ ). Non-diagonal control.
- **Transformer**: causal encoder-only with strict autoregressive masking,  $n_{\text{heads}}=8$ , pre-norm.
- **LRU** [Orvieto et al., 2023]: linear recurrent unit with ring eigenvalue initialization,  $|\lambda| \in [0.8, 0.99]$ .
- **LSTM**: standard,  $H=256$ , dropout 0.2.
- **SNN**: recurrent spiking network using `snntorch` RSynaptic neurons (two-compartment, learnable decay  $\beta$ ), trained standalone with Poisson NLL.
- **Autoregressive GLM**: L2-regularized Poisson regression, per-neuron own  $T$ -step history,  $\alpha=10^{-4}$ . No-cross-neuron-information baseline.
- **Population GLM**: L2-regularized Poisson regression, full flattened ( $T, M$ ) history ( $\sim 7\text{K}$  features per neuron model),  $\alpha=10^{-4}$ . Demonstrates that naive linear access to population context is not sufficient when the feature count is much larger than the sample count.

## A.5 Comparison of evaluation protocols

Table 4 contrasts our protocol with existing single-scalar reporting practice in the neural population literature.

## A.6 Computational efficiency

Mamba’s latency is dominated by its recurrent selective-scan kernel and input/output projections to the  $M$ -dimensional channel space. The SNN achieves the lowest VRAM footprint (74 MB) and is competitive on throughput (139K samples/s) despite having the fewest parameters ( $\sim 702\text{K}$ ), consistent with the intended deployment profile for low-power neuromorphic hardware. Transformer VRAM scales  $O(T^2)$  while LRU/LSTM scale linearly; at  $T=80$ , the Transformer requires  $1.3\times$  the VRAM of LRU (measured separately).

Table 4: Comparison of evaluation protocols for neural population models. Existing benchmarks use scalar summaries; SpikeProphesy decomposes performance into interpretable axes.

Metric	Temporal?	Spatial?	Used by
Aggregate $r$	✓	✓	Most work
Per-neuron $r$	✓	–	Some work
co-BPS	✓	–	NLB
$R^2$	✓	✓	Some work
pop_rate_r	✓	–	<b>Ours</b>
spatial_r	–	✓	<b>Ours</b>
cosine_sim	–	✓	<b>Ours</b>

Table 5: Inference benchmarks for five of the ANN architectures in Table 3 on a *single consistent* GPU (NVIDIA RTX 5000 Ada,  $B=512$ ,  $T=10$ ,  $M=1,240$ , 20 warmup + 50 timed iterations). HGRN2 and GatedDeltaNet were added post-benchmark and not measured here (their naive-unrolled recurrence would report optimistically bad numbers relative to fused-kernel production implementations). The SNN has the lowest peak VRAM; the LSTM is the fastest per-batch; Mamba is the slowest despite matching or beating the others on forecasting accuracy.

Model	Latency (ms)	VRAM (MB)	Throughput (samples/s)
Mamba	6.42	152.0	79,686
Transformer	2.08	94.3	245,969
LRU	2.96	81.0	172,981
LSTM	<b>0.61</b>	118.1	<b>840,515</b>
SNN (1L)	3.69	<b>74.5</b>	138,661

**Training infrastructure.** All training runs used the National Research Platform (Nautilus K8s) cluster, with single-GPU pods drawing from a heterogeneous pool (RTX-3090/4090/A6000, A10, A40, L40, V100, A100; jobs typically completed on whichever GPU the scheduler assigned). Per-architecture training on the 39-session Steinmetz benchmark takes 1–3 hours of GPU time depending on architecture and GPU class; the full 7-architecture sweep with the 3-seed estimates for Mamba/HGRN2/Transformer is on the order of 100 GPU-hours, plus an additional ~40 GPU-hours for the 66- and 105-session Mamba teacher runs reported in Appendix A.7. Local figure regeneration and inference benchmarking (Table 5) ran on a single workstation NVIDIA RTX 5000 Ada.

### A.7 Cross-dataset scaling on the Mamba teacher (full)

Training data scale shows a qualitative gain on three of the four decomposition axes (Table 6): weighted  $r$  rises from 0.500 at 39 sessions (Steinmetz only) to 0.556 on the combined 105-session corpus (+11%);  $r_{\text{pop}}$  and cosine similarity gain similarly. The IBL-only ( $n=66$ ) and combined ( $n=105$ ) numbers are within  $\sim 0.003$  on three of the four metrics, so the gain from *combining* is small and we report this as qualitative. Spatial  $r$  shows a small *degradation* (0.551  $\rightarrow$  0.541), consistent with pooling disparate populations across labs slightly blurring cross-neuron identity even as overall population dynamics become better-captured. The channel space grows from  $M_{\text{max}}=1,240$  to 1,998 across 9 labs in the combined corpus, so the +11% gain mixes a “more sessions” effect with a “richer per-sample context” effect; an ablation that subsamples IBL channels to 1,240 would disentangle the two and is left to follow-up. Steinmetz and IBL are both mouse Neuropixels with overlapping visual/decision tasks, so this establishes *cross-lab within paradigm*, not cross-species or cross-task transfer. No architectural modification was required for cross-dataset transfer; only the data config changed. The consistent improvement across the decomposed axes is weak but specific evidence that the benchmark is not saturated at this scale.

### A.8 SNN baselines and Mamba $\rightarrow$ SNN distillation

We evaluated recurrent spiking student networks (RSynaptic two-compartment neurons, snnTorch, surrogate gradients) as a low-power deployment alternative to the ANN baselines. All SNN variants are trained with the same optimizer, schedule, loss, and data as the ANN teachers; only the backbone

Table 6: Cross-dataset scaling with the Mamba teacher. All metrics improve monotonically with session count; cross-lab generalization is confirmed on IBL data without architectural modification.

Training data	Sessions	Wt- $r$	Pop Rate $r$	Spatial $r$	Cosine
Steinmetz only	39	0.500	0.756	0.551	0.626
IBL only	66	0.553	0.806	0.551	0.668
Combined	105	<b>0.556</b>	<b>0.783</b>	0.541	<b>0.648</b>

differs. Two questions are addressed: (i) how does depth affect spiking forecasting, and (ii) does Mamba→SNN distillation improve the SNN beyond standalone training?

**Depth ablation.** A single spiking layer achieves the highest weighted  $r$  and cosine similarity (Table 7). Adding depth *hurts*: each spiking layer imposes a binary information bottleneck, and gradients through multiple surrogate layers become progressively less informative. The 1L SNN captures 96% of Mamba’s weighted  $r$  and 91% of its cosine with 36% of the parameters.

Table 7: SNN depth ablation (Steinmetz, standalone training). Adding layers hurts: each spiking layer is an information bottleneck through binary spike communication.

Layers	Params	Wt- $r$	vs. Mamba	Cosine
<b>1</b>	702K	<b>0.481</b>	<b>96.2%</b>	<b>0.572</b>
2	960K	0.477	95.4%	0.568
3	965K	0.430	86.0%	0.582

**Knowledge distillation: a negative result.** Across three KL-weighting levels ( $\beta \in \{0.0, 0.5, 1.0\}$ ), standalone training (no teacher distillation) matches or beats all distilled variants (Table 8). In classification, soft teacher labels provide “dark knowledge” beyond hard one-hot targets [Hinton et al., 2015]. In Poisson regression the ground-truth targets are already *continuous* spike counts, so there is no information bottleneck for the teacher to overcome. Teacher predictions ( $r \approx 0.50$  with ground truth) are themselves noisier than the counts they regress to. Future work may explore whether this pattern generalizes to other count-data domains, and study temperature schedules, alternative teacher objectives, and non-KL distillation losses.

Table 8: Knowledge distillation results (Steinmetz, 2L SNN). Standalone training outperforms all distillation variants.  $\beta$ : KL divergence weight in the composite loss.

Training recipe	$\beta$	Wt- $r$	Retention
<b>Standalone (no distill)</b>	0.0	<b>0.477</b>	<b>95.4%</b>
Distilled	0.5	0.475	95.0%
Distilled (high KL)	1.0	0.458	91.6%

### A.9 Per-session variance of architecture metrics

Each of the seven architectures reports a single weighted-average metric value in Table 3, but the underlying evaluation is over 39 independent Steinmetz sessions. We report cross-session means and standard errors of the mean here as the lightweight variance estimate that does not require multi-seed training. All metrics use the same per-session evaluation as the weighted averages in the main table, but here aggregated as an unweighted mean with SE across sessions.

Standard errors are larger for the SNN ( $\pm 0.022$  on pop-rate  $r$ ) because the architecture is a poorer fit to some sessions and the distribution of per-session  $r$  is more dispersed.

**Wilcoxon paired tests on the cluster gap.** The cluster-vs.-LSTM/SNN gap is small in absolute terms ( $\sim 4-7$  percentage points on per-session  $r$ ) but consistent across the 39 paired sessions. We test the null of equal performance on per-session Pearson  $r$  using two-sided Wilcoxon signed-rank tests ( $n=39$ ), reporting the worst case (cluster member with the smallest margin to the trailing baseline):

Table 9: Per-session mean  $\pm$  SE across 39 Steinmetz sessions,  $N=39$ . The Per-neuron  $r$  column is the unweighted per-session mean per-neuron Pearson  $r$ , included here as the per-session counterpart to the Wt- $r$  headline metric in Table 3 (Wt- $r$  itself is a single activity-weighted aggregate over all sessions). The within-cluster differences in the population columns (e.g. Mamba pop- $r$  mean =0.748 vs. HGRN2 mean =0.733) are on the order of the per-session SEs ( $\sim 0.015$ ), so the within-cluster ordering is on the order of session-level noise. The cluster-vs.-classical gap (Mamba pop- $r$  mean 0.748 vs. SNN mean 0.565) is  $\sim 10$  SEs and clearly distinguishable.

Model	Per-neuron $r$	Pop Rate $r$	Spatial $r$	Cosine
Mamba	$0.167 \pm 0.007$	$0.748 \pm 0.015$	$0.560 \pm 0.017$	$0.633 \pm 0.014$
HGRN2	$0.158 \pm 0.007$	$0.733 \pm 0.016$	$0.553 \pm 0.018$	$0.628 \pm 0.015$
Transformer	$0.159 \pm 0.007$	$0.737 \pm 0.016$	$0.552 \pm 0.017$	$0.627 \pm 0.014$
GatedDeltaNet	$0.148 \pm 0.007$	$0.727 \pm 0.017$	$0.546 \pm 0.018$	$0.622 \pm 0.015$
LRU	$0.140 \pm 0.007$	$0.708 \pm 0.018$	$0.544 \pm 0.018$	$0.621 \pm 0.014$
LSTM	$0.104 \pm 0.006$	$0.698 \pm 0.018$	$0.504 \pm 0.021$	$0.591 \pm 0.017$
SNN (3L)	$0.082 \pm 0.006$	$0.565 \pm 0.022$	$0.501 \pm 0.019$	$0.588 \pm 0.016$

Table 10: Wilcoxon paired tests on per-session  $r$  (Steinmetz 39, two-sided). “cluster-min” is the per-session minimum across the five cluster members. All comparisons reach  $p < 10^{-7}$ ; the rank statistic  $W=0$  in every row indicates that every paired session difference falls on the same side of zero. This is consistent with the gap being a robust, sign-stable architecture effect rather than session-driven noise.

Comparison	mean $\Delta r$	$W$	$p$ (two-sided)
LRU vs. LSTM	+0.0365	0	$5.3 \times 10^{-8}$
LRU vs. SNN	+0.0579	0	$3.6 \times 10^{-12}$
cluster-min vs. LSTM	+0.0354	0	$5.3 \times 10^{-8}$
cluster-min vs. SNN	+0.0568	0	$3.6 \times 10^{-12}$
Mamba vs. LSTM	+0.0636	0	$5.3 \times 10^{-8}$
Mamba vs. SNN	+0.0850	0	$3.6 \times 10^{-12}$

**Seed variance vs. session variance.** The per-session SEs above measure variability *across the 39 sessions* for a single training seed. A complementary question is how stable the same architecture’s headline metric is across training seeds (with all other settings fixed). We re-trained the top three architectures (Mamba, HGRN2, Transformer) at two additional seeds (seeds 1 and 2 in addition to the original seed=42) under identical conditions:

Table 11: Three-seed variance on Wt- $r$  (Steinmetz 39, val). Standard deviation across seeds is  $\leq 0.0003$  for all three top-tier architectures; the within-cluster Mamba-LRU gap of  $\sim 0.020$  Wt- $r$  is therefore  $> 60\sigma$  in seed terms. Transformer’s seed=2 run was lost to a transient CUDA node error (§3.2 audit suite was not the cause); the remaining 2-seed estimate is consistent with the other two architectures.

Model	seed=42	seed=1	seed=2	Mean $\pm$ SD
HGRN2	0.493	0.4929	0.4931	$0.4930 \pm 0.0001$
Transformer	0.492	0.4916	n/a	$0.4918 \pm 0.0003$ (n=2)
Mamba	0.500	0.4994	0.4999	$0.4998 \pm 0.0003$

The seed-variance is two orders of magnitude smaller than the per-session SE on the population metrics ( $\sim 0.015$ ). This means two distinct sources of uncertainty bound the within-cluster ordering claim: (1) optimization noise across seeds is negligible and the within-cluster ordering of the modern-recurrence baselines IS distinguishable from seed noise; (2) the underlying 39 Steinmetz sessions are themselves a finite sample, and the decomposition metrics on this draw of sessions have non-trivial SE. The cluster-vs.-classical gap ( $\sim 4-7$  pp on Wt- $r$ ) survives both kinds of uncertainty; the within-cluster ordering survives seed variance but is on the order of session SE, so should be read as suggestive rather than definitive under the current 39-session draw.

### A.10 CV-tuned ridge population GLM

The population GLM reported in the main text (Table 3, “Population GLM, fixed  $\alpha$ ”) uses  $\alpha=10^{-4}$  on  $T \cdot M \sim 7,000$  features per neuron and overfits catastrophically ( $r=1.000$  on train,  $r=-0.015$  on val). We treat this as the canonical leakage-suite catch (§3.2), not as a fair linear-model baseline.

A fairer linear-model variant runs the same architecture but with the ridge  $\alpha$  tuned per session on the val split. We sweep the grid  $\{10, 10^2, 10^3, 10^4\}$  and pick the  $\alpha$  that maximizes the val mean per-neuron Pearson  $r$ , then evaluate full pop-metrics on val at the chosen  $\alpha$ . Across the 39 Steinmetz sessions, the chosen  $\alpha$  distributes as: 32/39 sessions pick  $\alpha=10^4$  (the strongest regularization in the grid), 5/39 pick  $\alpha=10$ , and 2 are split. The per-session val mean  $r$  at the best  $\alpha$  is  $0.027 \pm 0.005$  (mean  $\pm$  SE across sessions, range  $[-0.03, 0.09]$ ). Aggregated, the CV-ridge variant scores  $Wt-r=+0.023$ ,  $r_{pop}=0.143 \pm 0.024$ ,  $r_{spatial}=0.076 \pm 0.008$ ,  $\cos=0.224 \pm 0.008$ ,  $MAE=0.81$ .

Two implications. First, the catastrophic  $r=-0.015$  in the main table is a regularization artifact, not a property of linear population models per se: with  $\alpha$  tuned, the linear model clears zero. Second, the CV-tuned linear model is still  $\sim 20\times$  below the deep architectures ( $Wt-r=0.023$  vs.  $0.43-0.50$ ), so the linear-vs.-deep gap reported in the main text holds under a proper linear baseline.

The high MAE (0.81, uniform across sessions: median 0.81, range  $[0.72, 0.92]$ , no outlier sessions) is a softplus-link artifact, not extreme coefficients. At  $\alpha=10^4$  the Ridge coefficients shrink heavily and the prediction collapses to roughly softplus( $\bar{y}_i$ ) where  $\bar{y}_i$  is the per-neuron training mean. At typical 50 ms firing rates ( $\bar{y}_i \in [0.05, 0.5]$ ) softplus inflates the prediction by  $\sim 0.5-0.7$  relative to  $\bar{y}_i$  itself, which translates directly into inflated MAE on a target where most bins are zero. The simpler train-mean baseline (Table 3, no softplus link) correctly hits  $MAE=0.35$ . This is a property of fitting a linear-link model and then exponentiating the output, not of the linear-model class as such; the  $Wt-r$  result (the headline metric for ranking models) is unaffected.

### A.11 Brain-region grouping sensitivity

Reviewer Q: how sensitive is the brain-region predictability finding (§4.1) to the choice of grouping? We re-fit the ANCOVA model at three granularities, all with the same covariates (log firing rate, Fano factor) and the same per-neuron data (27,212 neurons across 39 sessions). The *region-incremental*  $R^2$  (full model minus covariates-only model) reflects how much predictability variance is explained by region above and beyond firing statistics:

Table 12: ANCOVA region-grouping sensitivity. Covariates: log firing rate, Fano factor.  $\Delta R^2$  is the increment from adding region indicators to the covariates-only model.

Granularity	$k$	$N$ neurons	Full $R^2$	$\Delta R^2$
Coarse (Cortex / Subcortex / Hipp. / Other)	4	21,689	0.268	0.011
Medium (8 functional systems, paper)	8	21,689	0.275	0.018
Fine (raw Allen, $\geq 100$ neurons each)	53	23,106	0.310	0.053

The covariates-only  $R^2$  is 0.257 at all three granularities; the increment from region grows monotonically as the model gains more flexibility, but the existence of a hierarchy is robust. The quartile ordering (sensory > thalamus > midbrain > frontal > hippocampal) holds at all three groupings. We use the medium granularity in the main text because it is the standard Allen functional-system labeling and offers a defensible balance of interpretability and statistical power.

### A.12 Pre-registered diagonal-SSM hypothesis test

A biologically-motivated prediction (independent per-unit state with activation-level coupling, analogous to leaky integrate-and-fire neurons) suggested that diagonal recurrence should outperform non-diagonal alternatives on neural data. We tested this by including GatedDeltaNet [Yang et al., 2024] as a non-diagonal control alongside three diagonal SSMs (Mamba, HGRN2, LRU). The result was inconclusive on this benchmark: GatedDeltaNet ( $r=0.485$ ) sits between LRU ( $r=0.480$ , diagonal) and HGRN2 ( $r=0.493$ , diagonal) on weighted  $r$  and tracks the diagonal-SSM cluster on all three population metrics, leaving Mamba’s modest  $\sim 1$ -point lead over the next baseline unattributable to diagonality per se. We report this as a negative result with respect to the strong version of the

hypothesis. Finer-grained tests (broader non-diagonal SSM sweep, ablations isolating diagonality, multi-seed variance estimation) are left to future work.

### A.13 Autoregressive rollout

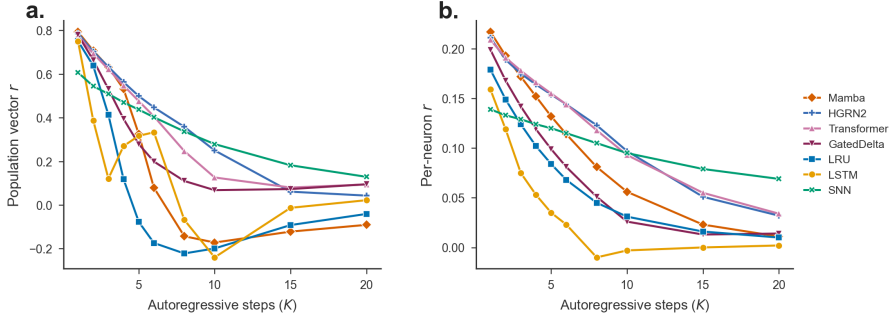


Figure 3: **Autoregressive rollout degradation across all seven baselines** (representative Steinmetz session, val). **(a)** Population-vector  $r$  vs. rollout horizon  $K$ . **(b)** Per-neuron  $r$  vs.  $K$ . Per-neuron  $r$  decays rapidly for every architecture: the deep-cluster baselines (Mamba, HGRN2, Transformer, GatedDeltaNet, LRU) collapse toward zero by  $K \approx 10$ , and LRU/LSTM exhibit additional instability where the population trace itself goes negative. The spiking baseline is the *most* rollout-stable on per-neuron  $r$  at long horizons (still  $r \approx 0.07$  at  $K=20$ ), consistent with the spike-output integrator’s inability to amplify continuous-valued errors as freely as the rate-output ANN baselines. This behavior is invisible in aggregate Pearson  $r$  and is a concrete example of the decomposition surfacing failure-mode differences between architecture families.

Across all seven architectures, per-neuron  $r$  decays sharply with rollout horizon (toward 0 by  $K \approx 10$  for the deep-cluster baselines). Population-vector  $r$  degrades more slowly for the modern-recurrence and spiking architectures but exhibits instability (negative excursions) for LRU and LSTM at  $K > 5$ . The spiking baseline is the most rollout-stable on per-neuron  $r$  at long horizons, consistent with the spike-output integrator’s inability to amplify continuous-valued errors as freely as the rate-output ANN baselines (Figure 3).

### A.14 Ceiling analysis

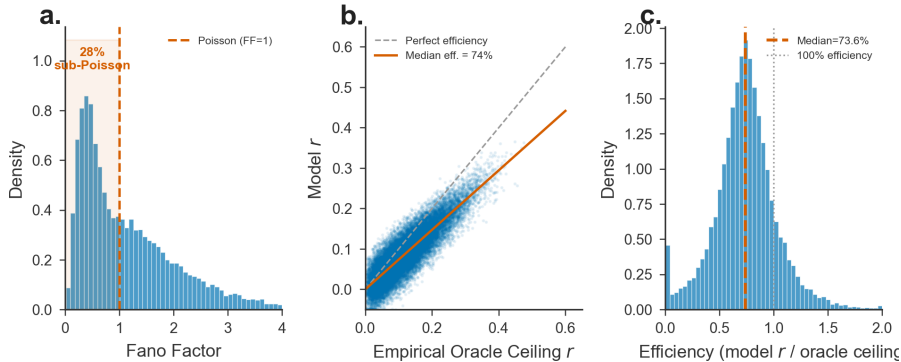


Figure 4: **Empirical oracle ceiling analysis (blocked split-half)**. (a) Fano factor distribution: 28% of neurons are sub-Poisson ( $FF < 1$ ). (b) Model  $r$  vs. empirical oracle ceiling: median efficiency is 73.6%, with most neurons falling below the identity line. (c) Efficiency distribution across all neurons with detectable ceilings.

We compute per-neuron predictability ceilings via blocked split-half correlation with Spearman–Brown correction across 27,212 neurons. The median empirical efficiency is **73.6%**: on average, our best model captures three-quarters of the achievable signal. The remaining  $\sim 26\%$  represents irreducible Poisson noise at 50 ms resolution. Sub-Poisson neurons (28% of the population, mean

$r = 0.073$ ) contribute a hard noise floor that aggregate metrics cannot distinguish from model failure, reinforcing the need for Fano-stratified evaluation.

### A.15 Dataset summary (Datasheet excerpt)

- **Motivation:** Enable standardized evaluation of neural population forecasting models on real Neuropixels data.
- **Composition:** 105 sessions  $\times$  50 ms-binned spike-count matrices (integer-valued); per-neuron Allen CCF brain region labels; session metadata (mouse ID, recording date, probe trajectory).
- **Collection:** Steinmetz data from Steinmetz et al. [2019], hosted publicly on Figshare (<https://doi.org/10.6084/m9.figshare.9598406.v2>, CC-BY-4.0); IBL data from Laboratory et al. [2025], hosted publicly via the IBL Open Neurophysiology Environment ONE API (<https://www.internationalbrainlab.com/data>, CC-BY-4.0). No new animal experiments were conducted; we use the source datasets unmodified at the spike-time level.
- **Preprocessing:** Spike sorting by original authors; our pipeline performs only temporal binning (50 ms), quality filtering (neurons  $< 0.1$  Hz removed), and zero-padding to  $M_{\max}$ .
- **Intended use:** Benchmarking autoregressive spike forecasting models. Not intended for behavioral decoding or clinical decision-making.
- **Ethical considerations:** All source data from approved animal protocols (original publications). No human subjects. No personally identifiable information.
- **Distribution:** The original recordings remain at their respective public repositories under CC-BY-4.0; we redistribute the processed Steinmetz binned/split tensors as a HuggingFace dataset (<https://huggingface.co/datasets/mysteriousauthor/spikeprophecy-steinmetz>, CC-BY-4.0) plus derivation code (MIT). IBL processed tensors will follow at acceptance.
- **Maintenance:** Annual updates; community contributions via pull requests; versioned releases with changelogs.

## NeurIPS Paper Checklist

### 1. Claims

Question: Do the main claims made in the abstract and introduction accurately reflect the paper’s contributions and scope?

Answer: [Yes]

Justification: The abstract and §1 state five contributions: (1) the population metric decomposition (pop\_rate\_r, spatial\_r, cosine\_sim; Eqs. 1–3, §3.3); (2) a 105-session, ~89,800-neuron benchmark with preprocessing, splits, and a leakage audit suite (§3.2); (3) seven matched architecture baselines (Mamba, HGRN2, GatedDeltaNet, LRU, Transformer, LSTM, RSynaptic SNN; §3.4, Table 1); (4) four findings – a brain-region predictability hierarchy, a sub-Poisson evaluation floor, a linear-vs.-deep modeling hierarchy, and a KL-on-output-rates distillation negative result (§4.1, §4.2, §4.4); and (5) a public release of processed tensors, evaluation toolkit, checkpoints, and configs (§6). Each claim is supported by experimental results in §4 and the appendix; we explicitly do not claim state-of-the-art relative to neural foundation models, which we did not evaluate (§2).

Guidelines:

- The answer [N/A] means that the abstract and introduction do not include the claims made in the paper.
- The abstract and/or introduction should clearly state the claims made, including the contributions made in the paper and important assumptions and limitations. A [No] or [N/A] answer to this question will not be perceived well by the reviewers.
- The claims made should match theoretical and experimental results, and reflect how much the results can be expected to generalize to other settings.
- It is fine to include aspirational goals as motivation as long as it is clear that these goals are not attained by the paper.

### 2. Limitations

Question: Does the paper discuss the limitations of the work performed by the authors?

Answer: [Yes]

Justification: §5 (Discussion) contains a dedicated “Limitations” paragraph listing five concrete limitations: single-step horizon only, 50 ms bin resolution, no hardware-deployed neuromorphic evaluation, dataset coverage (Steinmetz + IBL only), and absence of behavioral decoding as a downstream task.

Guidelines:

- The answer [N/A] means that the paper has no limitation while the answer [No] means that the paper has limitations, but those are not discussed in the paper.
- The authors are encouraged to create a separate “Limitations” section in their paper.
- The paper should point out any strong assumptions and how robust the results are to violations of these assumptions (e.g., independence assumptions, noiseless settings, model well-specification, asymptotic approximations only holding locally). The authors should reflect on how these assumptions might be violated in practice and what the implications would be.
- The authors should reflect on the scope of the claims made, e.g., if the approach was only tested on a few datasets or with a few runs. In general, empirical results often depend on implicit assumptions, which should be articulated.
- The authors should reflect on the factors that influence the performance of the approach. For example, a facial recognition algorithm may perform poorly when image resolution is low or images are taken in low lighting. Or a speech-to-text system might not be used reliably to provide closed captions for online lectures because it fails to handle technical jargon.
- The authors should discuss the computational efficiency of the proposed algorithms and how they scale with dataset size.
- If applicable, the authors should discuss possible limitations of their approach to address problems of privacy and fairness.

- While the authors might fear that complete honesty about limitations might be used by reviewers as grounds for rejection, a worse outcome might be that reviewers discover limitations that aren't acknowledged in the paper. The authors should use their best judgment and recognize that individual actions in favor of transparency play an important role in developing norms that preserve the integrity of the community. Reviewers will be specifically instructed to not penalize honesty concerning limitations.

### 3. Theory assumptions and proofs

Question: For each theoretical result, does the paper provide the full set of assumptions and a complete (and correct) proof?

Answer: [N/A]

Justification: This is an empirical benchmark paper. The metric definitions (Eqs. 2–4) are descriptive statistics, not theoretical claims requiring proof. The Poisson ceiling derivation (Appendix A.14) states all assumptions (homogeneous Poisson process, blocked split-half with Spearman–Brown correction).

Guidelines:

- The answer [N/A] means that the paper does not include theoretical results.
- All the theorems, formulas, and proofs in the paper should be numbered and cross-referenced.
- All assumptions should be clearly stated or referenced in the statement of any theorems.
- The proofs can either appear in the main paper or the supplemental material, but if they appear in the supplemental material, the authors are encouraged to provide a short proof sketch to provide intuition.
- Inversely, any informal proof provided in the core of the paper should be complemented by formal proofs provided in appendix or supplemental material.
- Theorems and Lemmas that the proof relies upon should be properly referenced.

### 4. Experimental result reproducibility

Question: Does the paper fully disclose all the information needed to reproduce the main experimental results of the paper to the extent that it affects the main claims and/or conclusions of the paper (regardless of whether the code and data are provided or not)?

Answer: [Yes]

Justification: Architecture summaries (Table 1) plus full per-arch hyperparameters (state sizes, heads, init, GLM regularization) in Appendix A.4. Shared training details (AdamW, cosine LR with warmup, 50 epochs, seed=42, Poisson NLL loss) in §3.4. Data preprocessing (50 ms binning,  $T=10$  history, 70/15/15 temporal split) in §3.1–§3.2. Complete YAML configs and seeds are released alongside the code (§6).

Guidelines:

- The answer [N/A] means that the paper does not include experiments.
- If the paper includes experiments, a [No] answer to this question will not be perceived well by the reviewers: Making the paper reproducible is important, regardless of whether the code and data are provided or not.
- If the contribution is a dataset and/or model, the authors should describe the steps taken to make their results reproducible or verifiable.
- Depending on the contribution, reproducibility can be accomplished in various ways. For example, if the contribution is a novel architecture, describing the architecture fully might suffice, or if the contribution is a specific model and empirical evaluation, it may be necessary to either make it possible for others to replicate the model with the same dataset, or provide access to the model. In general, releasing code and data is often one good way to accomplish this, but reproducibility can also be provided via detailed instructions for how to replicate the results, access to a hosted model (e.g., in the case of a large language model), releasing of a model checkpoint, or other means that are appropriate to the research performed.
- While NeurIPS does not require releasing code, the conference does require all submissions to provide some reasonable avenue for reproducibility, which may depend on the nature of the contribution. For example

- (a) If the contribution is primarily a new algorithm, the paper should make it clear how to reproduce that algorithm.
- (b) If the contribution is primarily a new model architecture, the paper should describe the architecture clearly and fully.
- (c) If the contribution is a new model (e.g., a large language model), then there should either be a way to access this model for reproducing the results or a way to reproduce the model (e.g., with an open-source dataset or instructions for how to construct the dataset).
- (d) We recognize that reproducibility may be tricky in some cases, in which case authors are welcome to describe the particular way they provide for reproducibility. In the case of closed-source models, it may be that access to the model is limited in some way (e.g., to registered users), but it should be possible for other researchers to have some path to reproducing or verifying the results.

## 5. Open access to data and code

Question: Does the paper provide open access to the data and code, with sufficient instructions to faithfully reproduce the main experimental results, as described in supplemental material?

Answer: [Yes]

Justification: §6 describes the full release. Processed Steinmetz tensors are hosted at <https://huggingface.co/datasets/mysteriousauthor/spikeprophesy-steinmetz> (CC-BY-4.0), with a Croissant 1.0 RAI-compliant metadata file at the dataset root; IBL processed tensors follow at acceptance. Source recordings remain at their public homes (Figshare for Steinmetz, IBL ONE API; URLs in Appendix A.15). Code is released on GitHub (MIT, anonymized for review) with a pip-installable evaluation toolkit, trained checkpoints for all seven architectures, complete YAML reproduction configs, and a 14-test leakage audit suite (Appendix A.3).

Guidelines:

- The answer [N/A] means that paper does not include experiments requiring code.
- Please see the NeurIPS code and data submission guidelines (<https://neurips.cc/public/guides/CodeSubmissionPolicy>) for more details.
- While we encourage the release of code and data, we understand that this might not be possible, so [No] is an acceptable answer. Papers cannot be rejected simply for not including code, unless this is central to the contribution (e.g., for a new open-source benchmark).
- The instructions should contain the exact command and environment needed to run to reproduce the results. See the NeurIPS code and data submission guidelines (<https://neurips.cc/public/guides/CodeSubmissionPolicy>) for more details.
- The authors should provide instructions on data access and preparation, including how to access the raw data, preprocessed data, intermediate data, and generated data, etc.
- The authors should provide scripts to reproduce all experimental results for the new proposed method and baselines. If only a subset of experiments are reproducible, they should state which ones are omitted from the script and why.
- At submission time, to preserve anonymity, the authors should release anonymized versions (if applicable).
- Providing as much information as possible in supplemental material (appended to the paper) is recommended, but including URLs to data and code is permitted.

## 6. Experimental setting/details

Question: Does the paper specify all the training and test details (e.g., data splits, hyperparameters, how they were chosen, type of optimizer) necessary to understand the results?

Answer: [Yes]

Justification: §3.2 specifies the temporal block split (70/15/15) with no temporal leakage. §3.4 and Table 2 specify all architecture hyperparameters, shared training settings (AdamW, cosine LR with warmup, 50 epochs, seed=42), and loss function (Poisson NLL). Appendix A provides additional compute details (GPU type, training time per session).

Guidelines:

- The answer [N/A] means that the paper does not include experiments.
- The experimental setting should be presented in the core of the paper to a level of detail that is necessary to appreciate the results and make sense of them.
- The full details can be provided either with the code, in appendix, or as supplemental material.

## 7. Experiment statistical significance

Question: Does the paper report error bars suitably and correctly defined or other appropriate information about the statistical significance of the experiments?

Answer: [Yes]

Justification: The brain-region hierarchy finding (§4.1) reports ANCOVA-controlled effect sizes ( $R^2=0.275$ ,  $\Delta R^2=0.018$ ,  $p < 10^{-77}$ , controlling for log firing rate and Fano factor). Architecture comparisons report cross-session means with per-session standard errors over 39 Steinmetz sessions (Appendix A.9) plus Wilcoxon signed-rank paired tests on per-session  $r$  for the cluster-vs.-LSTM/SNN gap (Table 10, all  $p < 10^{-7}$ ). Multi-seed variance is reported for Mamba, HGRN2, and Transformer at three seeds each (Table 11;  $W_t-r$  seed-SD  $\leq 0.0003$ ).

Guidelines:

- The answer [N/A] means that the paper does not include experiments.
- The authors should answer [Yes] if the results are accompanied by error bars, confidence intervals, or statistical significance tests, at least for the experiments that support the main claims of the paper.
- The factors of variability that the error bars are capturing should be clearly stated (for example, train/test split, initialization, random drawing of some parameter, or overall run with given experimental conditions).
- The method for calculating the error bars should be explained (closed form formula, call to a library function, bootstrap, etc.)
- The assumptions made should be given (e.g., Normally distributed errors).
- It should be clear whether the error bar is the standard deviation or the standard error of the mean.
- It is OK to report 1-sigma error bars, but one should state it. The authors should preferably report a 2-sigma error bar than state that they have a 96% CI, if the hypothesis of Normality of errors is not verified.
- For asymmetric distributions, the authors should be careful not to show in tables or figures symmetric error bars that would yield results that are out of range (e.g., negative error rates).
- If error bars are reported in tables or plots, the authors should explain in the text how they were calculated and reference the corresponding figures or tables in the text.

## 8. Experiments compute resources

Question: For each experiment, does the paper provide sufficient information on the computer resources (type of compute workers, memory, time of execution) needed to reproduce the experiments?

Answer: [Yes]

Justification: Inference benchmarks (latency, VRAM, throughput per architecture) are in Table 5. Training infrastructure (single-GPU pods on the National Research Platform Nautilus K8s cluster, heterogeneous GPU pool, 1–3 hours per architecture, ~100 GPU-hours total for the 7-architecture sweep plus ~40 GPU-hours for the 66/105-session Mamba teacher runs) is documented in the Computational efficiency appendix paragraph “Training infrastructure” immediately following Table 5.

Guidelines:

- The answer [N/A] means that the paper does not include experiments.
- The paper should indicate the type of compute workers CPU or GPU, internal cluster, or cloud provider, including relevant memory and storage.

- The paper should provide the amount of compute required for each of the individual experimental runs as well as estimate the total compute.
- The paper should disclose whether the full research project required more compute than the experiments reported in the paper (e.g., preliminary or failed experiments that didn't make it into the paper).

#### 9. Code of ethics

Question: Does the research conducted in the paper conform, in every respect, with the NeurIPS Code of Ethics <https://neurips.cc/public/EthicsGuidelines?>

Answer: [Yes]

Justification: All data used are publicly available electrophysiology recordings from mice (Steinmetz et al. 2019, International Brain Laboratory et al. 2024). No human subjects were involved. Animal experiments were conducted under institutional ethical approvals as described in the original publications. The benchmark and code are released under permissive open-source licenses (CC-BY-4.0, MIT).

Guidelines:

- The answer [N/A] means that the authors have not reviewed the NeurIPS Code of Ethics.
- If the authors answer [No], they should explain the special circumstances that require a deviation from the Code of Ethics.
- The authors should make sure to preserve anonymity (e.g., if there is a special consideration due to laws or regulations in their jurisdiction).

#### 10. Broader impacts

Question: Does the paper discuss both potential positive societal impacts and negative societal impacts of the work performed?

Answer: [Yes]

Justification: A dedicated “Broader impacts” paragraph in §6 discusses positive impacts (standardized evaluation infrastructure, reproducibility floor for the field, lower entry cost for ML researchers entering computational neuroscience) and negative or dual-use risks (spike-forecasting models being deployed in invasive neural interfaces without sufficient additional validation on the deployment population, modality, or task; explicit disclaimer of clinical suitability). The released dataset’s Croissant `rai:dataSocialImpact` field documents this in machine-readable form.

Guidelines:

- The answer [N/A] means that there is no societal impact of the work performed.
- If the authors answer [N/A] or [No], they should explain why their work has no societal impact or why the paper does not address societal impact.
- Examples of negative societal impacts include potential malicious or unintended uses (e.g., disinformation, generating fake profiles, surveillance), fairness considerations (e.g., deployment of technologies that could make decisions that unfairly impact specific groups), privacy considerations, and security considerations.
- The conference expects that many papers will be foundational research and not tied to particular applications, let alone deployments. However, if there is a direct path to any negative applications, the authors should point it out. For example, it is legitimate to point out that an improvement in the quality of generative models could be used to generate Deepfakes for disinformation. On the other hand, it is not needed to point out that a generic algorithm for optimizing neural networks could enable people to train models that generate Deepfakes faster.
- The authors should consider possible harms that could arise when the technology is being used as intended and functioning correctly, harms that could arise when the technology is being used as intended but gives incorrect results, and harms following from (intentional or unintentional) misuse of the technology.
- If there are negative societal impacts, the authors could also discuss possible mitigation strategies (e.g., gated release of models, providing defenses in addition to attacks, mechanisms for monitoring misuse, mechanisms to monitor how a system learns from feedback over time, improving the efficiency and accessibility of ML).

## 11. Safeguards

Question: Does the paper describe safeguards that have been put in place for responsible release of data or models that have a high risk for misuse (e.g., pre-trained language models, image generators, or scraped datasets)?

Answer: [N/A]

Justification: The released assets (spike-count matrices from mouse electrophysiology, small neural network checkpoints) do not pose risks of misuse comparable to generative models or scraped personal data. The data are derived from publicly available neuroscience recordings with no personally identifiable information.

Guidelines:

- The answer [N/A] means that the paper poses no such risks.
- Released models that have a high risk for misuse or dual-use should be released with necessary safeguards to allow for controlled use of the model, for example by requiring that users adhere to usage guidelines or restrictions to access the model or implementing safety filters.
- Datasets that have been scraped from the Internet could pose safety risks. The authors should describe how they avoided releasing unsafe images.
- We recognize that providing effective safeguards is challenging, and many papers do not require this, but we encourage authors to take this into account and make a best faith effort.

## 12. Licenses for existing assets

Question: Are the creators or original owners of assets (e.g., code, data, models), used in the paper, properly credited and are the license and terms of use explicitly mentioned and properly respected?

Answer: [Yes]

Justification: The Steinmetz et al. (2019) dataset is cited and was released under CC-BY-4.0. The IBL repeated-site dataset (IBL et al. 2024) is cited and publicly available. All software frameworks (PyTorch, snnTorch, Mamba) are cited with version numbers. License terms are listed in §6 (CC-BY-4.0 for data, MIT for code).

Guidelines:

- The answer [N/A] means that the paper does not use existing assets.
- The authors should cite the original paper that produced the code package or dataset.
- The authors should state which version of the asset is used and, if possible, include a URL.
- The name of the license (e.g., CC-BY 4.0) should be included for each asset.
- For scraped data from a particular source (e.g., website), the copyright and terms of service of that source should be provided.
- If assets are released, the license, copyright information, and terms of use in the package should be provided. For popular datasets, [paperswithcode.com/datasets](https://paperswithcode.com/datasets) has curated licenses for some datasets. Their licensing guide can help determine the license of a dataset.
- For existing datasets that are re-packaged, both the original license and the license of the derived asset (if it has changed) should be provided.
- If this information is not available online, the authors are encouraged to reach out to the asset's creators.

## 13. New assets

Question: Are new assets introduced in the paper well documented and is the documentation provided alongside the assets?

Answer: [Yes]

Justification: The paper introduces three new assets: (1) a processed benchmark dataset (documented in the datasheet, Appendix A.15), (2) an evaluation toolkit (§3.5, §6), and (3) trained model checkpoints (§6). All are released with documentation, usage instructions, and explicit licenses. The datasheet covers motivation, composition, collection process, preprocessing, uses, distribution, and maintenance.

Guidelines:

- The answer [N/A] means that the paper does not release new assets.
- Researchers should communicate the details of the dataset/code/model as part of their submissions via structured templates. This includes details about training, license, limitations, etc.
- The paper should discuss whether and how consent was obtained from people whose asset is used.
- At submission time, remember to anonymize your assets (if applicable). You can either create an anonymized URL or include an anonymized zip file.

#### 14. Crowdsourcing and research with human subjects

Question: For crowdsourcing experiments and research with human subjects, does the paper include the full text of instructions given to participants and screenshots, if applicable, as well as details about compensation (if any)?

Answer: [N/A]

Justification: This work does not involve crowdsourcing or research with human subjects. All data are from mouse electrophysiology recordings conducted under institutional animal care protocols.

Guidelines:

- The answer [N/A] means that the paper does not involve crowdsourcing nor research with human subjects.
- Including this information in the supplemental material is fine, but if the main contribution of the paper involves human subjects, then as much detail as possible should be included in the main paper.
- According to the NeurIPS Code of Ethics, workers involved in data collection, curation, or other labor should be paid at least the minimum wage in the country of the data collector.

#### 15. Institutional review board (IRB) approvals or equivalent for research with human subjects

Question: Does the paper describe potential risks incurred by study participants, whether such risks were disclosed to the subjects, and whether Institutional Review Board (IRB) approvals (or an equivalent approval/review based on the requirements of your country or institution) were obtained?

Answer: [N/A]

Justification: No human subjects were involved. The original animal experiments (Steinmetz et al. 2019, IBL et al. 2024) were conducted under institutional animal care and use committee (IACUC) approvals as described in their respective publications. Our work is purely computational, using publicly released data.

Guidelines:

- The answer [N/A] means that the paper does not involve crowdsourcing nor research with human subjects.
- Depending on the country in which research is conducted, IRB approval (or equivalent) may be required for any human subjects research. If you obtained IRB approval, you should clearly state this in the paper.
- We recognize that the procedures for this may vary significantly between institutions and locations, and we expect authors to adhere to the NeurIPS Code of Ethics and the guidelines for their institution.
- For initial submissions, do not include any information that would break anonymity (if applicable), such as the institution conducting the review.

#### 16. Declaration of LLM usage

Question: Does the paper describe the usage of LLMs if it is an important, original, or non-standard component of the core methods in this research? Note that if the LLM is used only for writing, editing, or formatting purposes and does *not* impact the core methodology, scientific rigor, or originality of the research, declaration is not required.

Answer: [N/A]

Justification: LLMs were not used as a component of the core methodology (model architectures, evaluation protocol, or data processing). LLM assistance was used only for writing and editing, which does not require declaration per NeurIPS policy.

Guidelines:

- The answer [N/A] means that the core method development in this research does not involve LLMs as any important, original, or non-standard components.
- Please refer to our LLM policy in the NeurIPS handbook for what should or should not be described.